AIMS Energy, 7(6): 710–727.
DOI: 10.3934/energy.2019.6.710
Received: 29 May 2019
Accepted: 17 September 2019
Published: 11 November 2019

http://www.aimspress.com/journal/energy

Research article

Estimation of clear sky global solar radiation in Algeria

Djelloul Benatiallah[1,*], Ali Benatiallah[1], Kada Bouchouicha[2] and Bahous Nasri[1]

[1] Laboratory of Energy Environment and Information System (LEEIS), Department of material sciences, university of Ahmed Draia, street 11 December 1960, Adrar (01000), Algeria
[2] Unité de recherche en énergie renouvelables en milieu Saharien (URERMS), Centre de Développement des Energies Renouvelables (CDER), 01000 Adrar, Algérie

*** Correspondence**: Email: djelloulunv@gmail.com; Tel: +213662117903.

Abstract: The paper presents the evaluation of performance of three models at three sites for estimating instantaneous clear-sky global solar radiation on a horizontal surface in Algeria. Additionally, recommend it to be used for estimating solar radiation at many locations in similar climates where radiometric measurements are not available and which might be helpful in the selection of the most suitable locations for solar power installations. The results in general exhibit that for global radiation, the daily correlation coefficient is higher than 0.99, whereas the mean absolute percentage error is less than 5%. The daily mean bias error ranges between −3 and +3%. The daily root mean square error is less than 7%. These results represent a precision that indicates that Atwater & Ball and Bird & Hulstrom models can be used successfully to predict solar radiation over three stations in the studied sites.

Keywords: Evaluation; global radiation; clear-sky; horizontal surface; radiometric measurements

Abbreviations: G: Global radiation (W/m^2); I: Direct radiation (W/m^2); D: Diffuse radiation (W/m^2); In: Direct normal radiation (W/m^2); h: Solar elevation (degrees); I_0: Solar constant (W/m^2); θz: Zenith angle (degrees); τ_{aa} : Transmittance of direct radiation; m_a: Air mass (dimensionless); U_1: Pressure-corrected (cm); τ_r, τ_o, τ_g, τ_w, τ_a: Transmittances related to Rayleigh, ozone, gas, water, and aerosols scattering (dimensionless)

1. Introduction

In recent years, there has been an increasing interest in the demand for energy produced by oil, gas, and uranium. This growing would occur relatively quickly in order to use for heating, cooling and electricity generation. There is evidence that numerous natural sources have been destroyed during the past decades, especially oil and gas based fuels sources, due to the rapid development of industry applications [1]. In the global economy, a growing community of researcher focusing on the area of renewable energy including solar, wind and geothermal with the aim of providing energy in the future. Therefore, researchers have focused on various forms of renewable energy that can satisfy the world demand without adversely affecting the environment. Solar energy is widely available almost everywhere, it is safe, environmental friendly, and unlimited in many areas of the world as well as has an economic feasibility to supply the energy needs of the world [2]. In solar energy systems, solar radiation data are extremely vital and being used in design, evaluation, and optimisation of the performance of various solar energy technologies and field applications [3].There are several analyses reviewed by the PV system using the solar radiation estimations in India, Iran and Egypt [4–6] and in other countries in the world.

Furthermore, the solar radiation components on horizontal and inclined surfaces are considered an integral part of studies of solar system's performance [7]. However, the radiation measurements stations do not always provide enough geographical sites. Generally, in many parts of the world, the meteorological facilities for solar radiation assessment are either absent or scarce [8]. Consequently, they need to be estimated using solar radiation modelling, which requires the knowledge of the clear-sky atmospheric transmittance.

Many aspects of modelling approaches for estimation of clear-sky solar radiation were studied in the last few years. To date, several studies have investigated and developed different approaches for this purpose based on different sources of data [9–19]. The solar radiation depended on various meteorological and geographic variables such as air temperature, atmospheric pressure, humidity, and solar zenith [20–24]. Previous studies focused on the sunshine duration to estimate the solar radiation [25], and use the satellite data [26,27]. In addition, these studies models are formulated in similar forms and related to the sites when they can be validated with the actual measured values of the sites during different seasons [3]. The first main group is physical model, which focused on the use of radiative transfer equations [28–30]. These types of equations are based on complex solves solutions and therefore required very specific mathematical tool which simultaneously solve a large dataset. The second group is the parametrical model [31–34], which has the same physical principles as the previous group with a set of simplified parameters. The parametric model improved the transmittance expression for the different attenuation processes in the atmosphere, which can be further used to estimate the direct component of incoming solar radiation. The diffuse radiation was calculated based on some approximations to reduce the complexity of the scattering process. Hence, global radiation was produced by combining the direct and diffuse horizontal radiations [35]. The previous models were evaluated only in few cities in the world, it is necessary to estimate daily data on global solar radiation for other cities such as the southern of Algeria.

The purpose of this study is to determine the accuracy of the estimation of three models developed for the prediction of global solar radiation over a horizontal surface at three cities in the Algerian big Sahara; three of the most accurate models were investigated for clear skies solar radiation modelling. First, the model of Bird & Hulstrom [29] is considered as a reference for designers of solar

systems. This model takes into account the data's weather, including air temperature, humidity, and atmospheric pressure. In addition, the Second model of Ashrae [31] is a simpler model used in different types of solar energy applications and requires solar zenith angle and some empirical formulas. Finally, the third model of Atwater & Ball [33] is dependent on numerous atmospheric parameters and coefficients. These models were evaluated for estimation of instantaneous clear-sky solar radiation on a horizontal surface in the Algerian south climate through comparing measured data with estimated values. The verification and validation of the whole models were carried out after the continuously collection of radiometric and meteorological data from three locations; El-golea, Adrar and Tamanrasset which were situated in the central of Sahara region. The climate of the studied areas is continental desert with hot desert climate, long summers and short warm winters; the climate was characterized by a high variation of temperatures exceeding 45 ° between June and August and 18 ° between November and January. These regions also have tremendous solar energy potential as depicted in Figure 1, with high global solar radiation intensity, and sunshine duration ranged between 9 to 11 hours per day [36,37].

2. Data

The experimental data were collected from three different stations situated in the southern region of Algeria in solar active region where the latitude ranged from 22 ° to 31 °N, and longitude ranged from 1 °W to 6 °E [3]. Thus, ample sunlight is available which accounts for more than 3000 hours of sunshine per year with over 5.5 kWh/m^2/day of solar radiation intensity (Figure 1).

According to first station, the measurements of diffuse and global radiation was carried out in the Renewable Energies Research Unit situated in Saharan Medium (RERUSM) in the state of Adrar which consisted of SOLYS 2 system Kipp & Zonen CMP21 Pyranometer (Figure 2). The second station of El- golea was equipped with Kipp & Zonen CMP 6 Pyranometer. For the third station measurements was performed in the National Meteorological Office (NMO) in the state of Tamanrasset using Eppley PSP pyranometer. The characteristics of equipment used are included in Table 2. In the present study simple quality control procedures were adopted and conducted in order to improve the obtained results (data initially lacking or removed via quality checks) [38,39]. The physical limit of test processes were applied to the global solar irradiance using the horizontal surface values of extraterrestrial irradiance. According to the outcomes of quality controls, the missing measurements represent around 11%, 3% and 6% of the whole database for the first, the second, and the third stations, respectively.

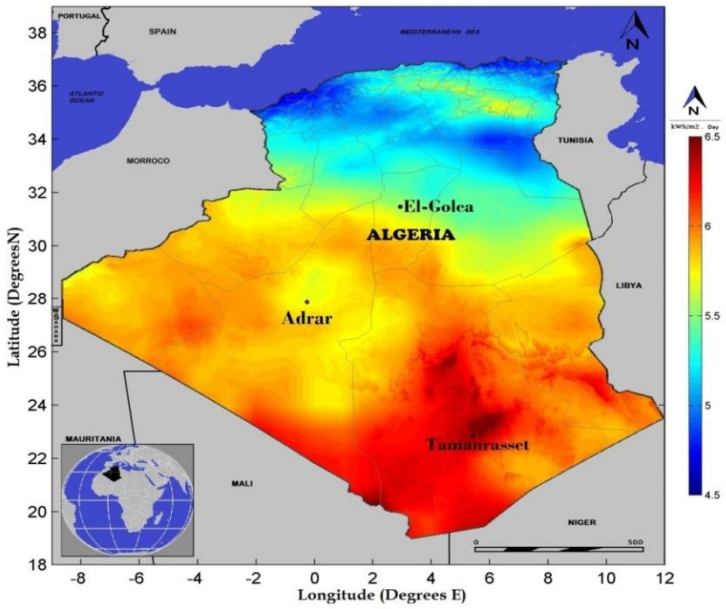

Figure 1. Map of annual average of global horizontal solar radiation in Algeria.

The data collection of this research performed in one year started from January to December 2016 with a datasets composed of 5 min as an averaged value for Adrar station, 1 min for Tamanrasset station, and 10 min for El-golé station, there are about 12,612 selected measurements in total.

Table 1. Geographical coordinates of selected sites.

Station	Sites	Longitude	Latitude	Altitude (m)
Station 1	Tamanrasset	5 °52’E	22°78’N	1320
Station 2	Adrar	0°28’W	27°88’N	269
Station 3	El Golé	2°87’E	30°58’N	380

Figure 2. Meteorological stations.

Table 2. Characteristics of solar instruments.

Sensor	Kipp & Zonen CMP21	Kipp & Zonen CMP 6	Eppley PSP
Maximum operational irradiance	4000 W/m^2	2000 W/m^2	4000 W/m^2
Spectral range	270 to 3000 nm	285 to 2800 nm	305–2800 nm
Sensitivity	7 to 14 μV/W/m^2	5–20 μV/W/m^2	7 mV/kW/m^2
Directional response	<10 W/m^2	<20 Wm^{-2}	< ±10 W/m^2
Non-stability (Change/year)	<0.5%	0.5%	< ±0,2%
Temperature response	<1% (−20 °to +50 °)	4% (0 °to +100 °)	< ±1%
Response time	<5 s	18 s	~8 sec
Non-linearity	<0.2 %	0.5%	< ±0,2%
Operating and storage temperature range	−40 °to +80 °	−40 °to +80 °	−40 °to +80 °

3. Methodology

The global radiation received by the sun is the sum of direct, diffuse radiation and reflected components. The reflected component has the null value in horizontal surface. Figure 3 depicts the constituents of the incoming solar radiation [40]. The global irradiance G (W/m^2) on a horizontal surface can be given by [43]:

$$G = I + D \tag{1}$$

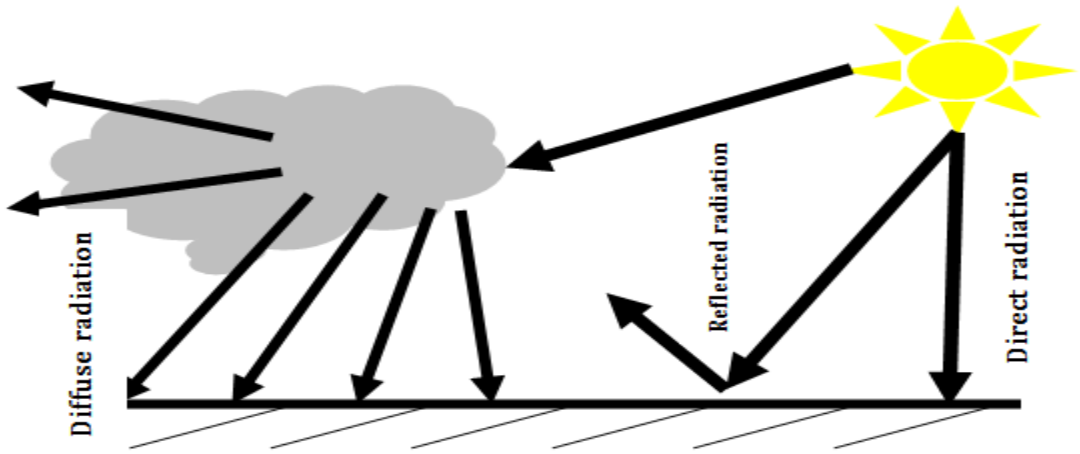

Figure 3. Components of global radiation.

The following subsection describes the investigated models as well as the techniques used to calculate fundamental equations and various parameters in horizontal surfaces.

3.1. Bird & Hulstrom model

Following the first model of Bird & Hulstrom, the direct normal irradiance in the direction of rays I_n (W/m^2) depends on absorption, transmittance, and atmospheric components which can be estimated using the following equation [41–43]:

$$I_n = 0.9751\, I_0 \tau_r \tau_g \tau_0 \tau_w \tau_a \quad (2)$$

where the factor of 0.9751 depended on the spectral range of 0.3–3 μm, I_0 is the solar constant (W/m^2); and h is the solar elevation (degrees). τ_r, τ_o, τ_g, τ_w, τ_a (dimensionless) are the transmittances related to Rayleigh, ozone, gas, water, and aerosols scattering.

These components are formulated respectively by:

$$\tau_r = \exp\left(-0.903 m_a^{0.84}\left(1 + m_a - m_a^{1.01}\right)\right) \quad (3)$$

$$\tau_0 = 1 - \left(0.1611 U_3 \left(1 + 139.48 U_3\right)^{-0.3035} - 0.002715 U_3 \left(1 + 0.044 U_3 + 0.0003 U_3^2\right)\right)^{-1} \quad (4)$$

$$\tau_g = \exp\left(-0.0127 m_a^{0.26}\right) \quad (5)$$

$$\tau_w = 1 - 2.4959 U_1 \left(\left(1 + 79.034 U_1\right)^{0.6828} + 6.385 U_1\right)^{-1} \quad (6)$$

$$\tau_a = \exp\left(-K_a^{0.873}\left(1 + K_a - K_a^{0.7808}\right) m_a^{0.9108}\right) \quad (7)$$

where m_a (dimensionless) is the air mass at actual pressure, U_1 (cm) is the pressure-corrected relative optical-path length of precipitable water, K_a represent the aerosol optical thickness, and U_3 (cm) is the ozone's relative optical path length. They are given by [43].

$$m_a = \frac{1}{\sin(h) + 9.4 \times 10^{-4} \left(\sin(h) + 0.0678\right)^{-1253}} \quad (8)$$

$$m_r = m_a \left(\frac{P}{1013.25}\right)^{-1} \quad (9)$$

$$U_1 = \frac{0.493}{T} HR \exp\left(26.23 - \frac{5416}{T}\right) \quad (10)$$

T, ambient temperature (K) and HR, relative humidity (%).

$$K_a = 0.2758\, K_{a\lambda/\lambda=0.38\mu m} + 0.35\, K_{a\lambda/\lambda=0.5\mu m} \quad (11)$$

$$K_a(\lambda) = \beta \lambda^{-\alpha} \quad (12)$$

λ (μm) is the wavelength, and β, α (dimensionless) are the Angstrom turbidity coefficients [44,45], and these are as follows in Table 3:

Table 3. Angstrom turbidity coefficient [43].

Zone climatic	β	α
Rural site	0.05	0.11
Urban site	0.10	0.22
Industrial site	0.30	0.66

$$U_3 = L\, m_r \quad (13)$$

$$L = \frac{1}{9.4 + 0.9\, m_a} \quad (14)$$

where, p (mbar) is the local air-pressure, z(m) is the altitude of studied position, L (cm) is the vertical ozone-layer thickness, m_r (dimensionless) is the air mass at standard pressure (1013.25 mbar) [46,47].

$$p = 1013\left(1 - 2.257 \times 10^{-5}\, Z\right)^{5.26} \quad (15)$$

$$T = 288 - 6.5 \text{ x } 10^{-3} Z \tag{16}$$

The beam irradiance I is illustrated by the following formula:

$$I = I_n \cos \theta_z \tag{17}$$

where θ_z (degrees) is the zenith angle.

In this model, the diffuse radiation D (W/m^2) in horizontal plane represents the sum of three diffuse components: the Rayleigh scattering component D_r; the aerosol component D_a; and the component that can be used for multiple reflections of irradiance between the ground and sky D_m. All these components are given in the following expressions.

$$D = D_r + D_a + D_m \tag{18}$$

$$D_r = \frac{0.79\, I_{sc}\ \sin(h)\ \tau_0 \tau_g \tau_w \tau_{aa}\ 0.5(1-\tau_r)}{1-m_a+m_a^{1.02}} \tag{19}$$

where I_{sc} is the correction of the solar constant, τ_{aa} is the transmittance of direct radiation due to aerosols absorption is given by the following expression:

$$\tau_{aa} = 1 - (1-\omega_0)(1 - m_a + m_a^{1.06})(1-\tau_a) \tag{20}$$

$$D_a = \frac{0.79\, I_{sc}\ \sin(h)\ \tau_0 \tau_g \tau_w \tau_{aa}\ F_c\ 0.5(1-\tau_{as})}{1-m_a+m_a^{1.02}} \tag{21}$$

where F_c is the coefficient of dispersion of the atmosphere. $F_c = 0.84$ is the value recommended by this model [48].

As explained in the following the T_{as} is the transmittance due to aerosol scattering.

$$\tau_{as} = \frac{\tau_a}{\tau_{aa}} \tag{22}$$

The multiple-reflection occurring between the ground and sky is accounted as follows:

$$D_m = \frac{(I_n \sin(h) + D_r + D_a)\rho_g\ \rho_a}{1-\rho_g\ \rho_a} \tag{23}$$

$$\rho_a = 0.0685 + (1-F_c)(1-\tau_{as}) \tag{24}$$

With ρ_g is the ground albedo and ρ_a is the clear sky albedo, h (degrees) is the solar elevation; and $\omega_0 = 0.9$ is the aerosol single of scattering albedo [49].

3.2. Ashrae model

Ashrae is an empirical model (model 2) used in many solar applications, depending on the solar zenith angle θ_z as well some empirical values A, B and C (see Table 4).The following equations explained the global solar irradiance G and the direct solar irradiance I_n as well as the diffuse solar irradiance D in horizontal plane [31], respectively.

$$G = I_n \cos \theta_z + D \tag{25}$$

$$I_n = A \exp(-B/\cos(\theta_z)) \tag{26}$$

$$D = C\, I_n \tag{27}$$

Table 4. A, B and C are the values of Ashrae model.

Month	A	B	C
Jan	1230	0.142	0.058
Feb	1215	0.144	0.060
Mar	1186	0.156	0.071
Apr	1136	0.180	0.097
May	1104	0.196	0.121
Jun	1088	0.205	0.134
Jul	1085	0.207	0.136
Aug	1107	0.201	0.122
Sep	1152	0.177	0.092
Oct	1193	0.160	0.073
Nov	1221	0.149	0.063
Dec	1234	0.142	0.057

3.3. Atwater And Ball Model

The model of Atwater & Ball (Model 3) demonstrated the relationship between precipitable water, pressure, air mass, together with broad band aerosol optical depth in order to calculate the aerosols and water vapor transmittances. The global solar radiation in horizontal surface and clear sky is explained by the following [33]:

$$G = I_0 \cos(\theta_z)\left((\tau_{md} - a_w)\tau_a/(1 - 0.0685\rho)\right) \tag{28}$$

where

$$\tau_{md} = 1.041 - 0.16\left(m_a(949 \times 10^{-6}p + 0.051)\right)^{0.5} \tag{29}$$

$$a_w = 0.077(U_1 m_a)^{0.3} \tag{30}$$

τ_{md} is the direct transmission coefficient while a_w is the absorption of solar radiation.

3.4. Statistical evaluation

The prediction performance of the considered models was assessed using parameters commonly used in statistical scores [44], such as Mean Bias Error (MBE), Root Mean Square Error (RMSE), Coefficient of correlation (R), and Relative Mean Absolute Percentage Error (MAPE).

These are specified by the following Eqs (31–36).

$$MBE = \frac{1}{K}\sum\left(G_c^i - G_m^i\right) \tag{31}$$

$$RMSE = \left(\frac{1}{K}\sum\left(G_c^i - G_m^i\right)^2\right)^{\frac{1}{2}} \tag{32}$$

$$MAPE = \frac{100}{K}\sum\left|\frac{\left(G_c^i - G_m^i\right)}{G_m^i}\right| \tag{33}$$

Relative Mean Absolute Percentage Error (MAPE) was considered to be acceptable by then less 10%.

$$R = \frac{\sum(G_c^i - \overline{G_c^i})(G_m^i - \overline{G_m^i})}{\sqrt{\sum(G_c^i - \overline{G_c^i})^2 \sum(G_m^i - \overline{G_m^i})^2}} \tag{34}$$

The relative MBE (rMBE) and relative RMSE (rRMSE) are calculated by the following:

$$rMBE = 100\left(\frac{1}{K}\sum\left(\frac{G_c^i - G_m^i}{G_m^i}\right)\right) \tag{35}$$

$$rRMSE = 100\left(\frac{1}{K}\sum\left(\frac{G_c^i - G_m^i}{G_m^i}\right)^2\right)^{\frac{1}{2}} \tag{36}$$

where G^i_c: is the i^{th} predicted value; G^i_m: is the i^{th} measured value; K: is the total number of evaluated data points.

4. Results and discussion

The main goal of the current study was to assess the solar radiation models and the comparison between measured and simulated values. Therefore, a proper computer programs using MATLAB® software were developed for clear skies solar radiation estimation in the three locations; Tamanrasset, Adrar and El-golea. The measurements data was collected in horizontal plane.

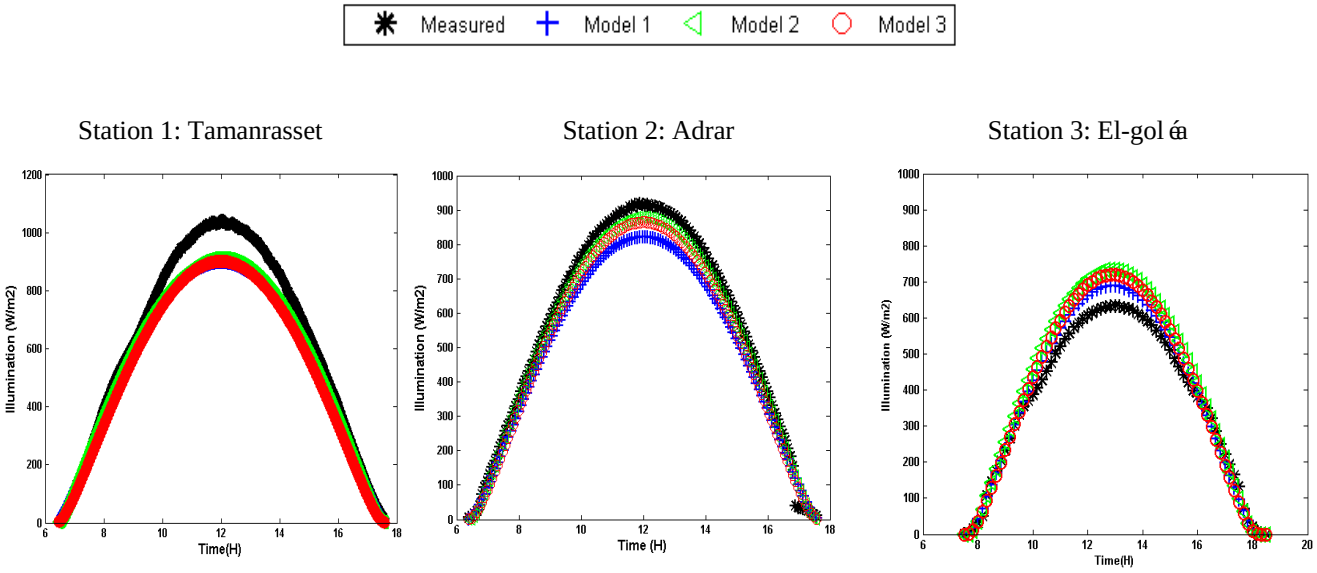

Figure 4. Global solar radiation fluxes on February 24, 2016.

The Figures 4–7 showed clearly the comparison between the predicted and the experimental value of global solar radiation flux during the year of 2016.

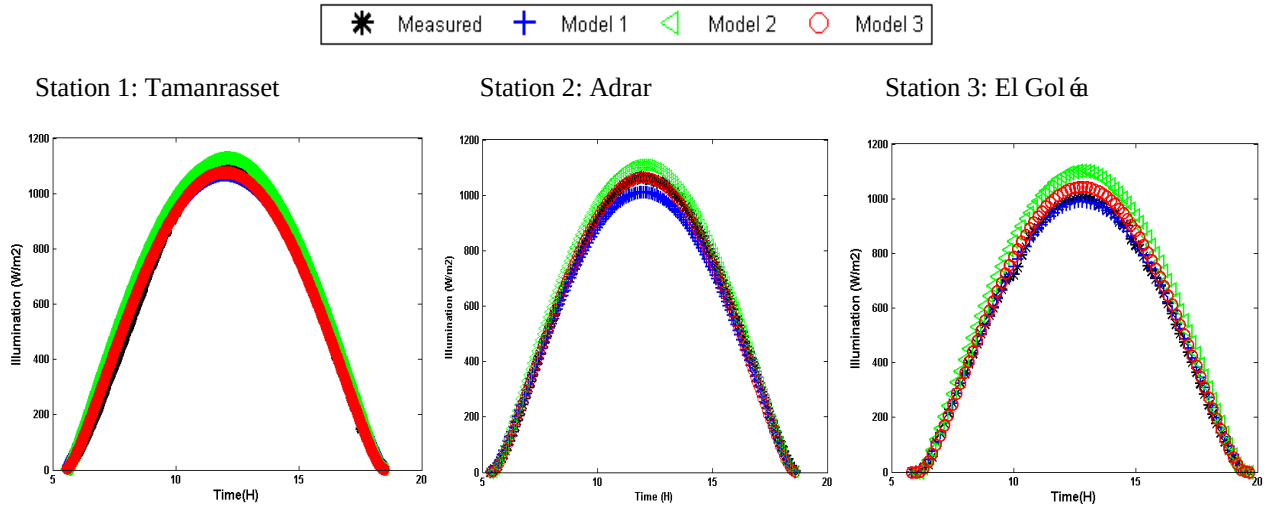

Figure 5. Global solar radiation fluxes on May 17, 2016.

The data in the following figure exhibited the measured values of global solar radiation in horizontal surface based on three models for the three locations named; Tamanrasset (station 1), Adrar (station 2), and El-golé a (station 3) with the comparison of the global solar radiation fluxes predicted by the studied models, Bird & Hulstrom (Model 1), Ashrae (Model 2), and Atwater & Ball (Model 3).

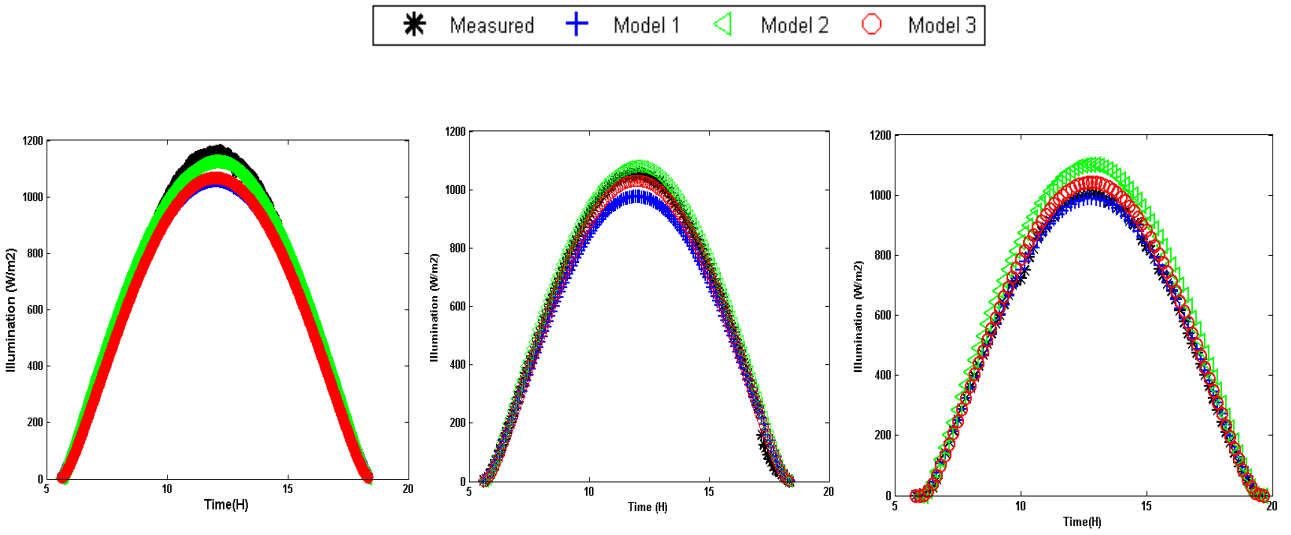

Figure 6. Global solar radiation fluxes on August 03, 2016.

The Figures 4–7 illustrated the comparison of results between the predicted and measured values recorded in three different stations in the Algerian southern.

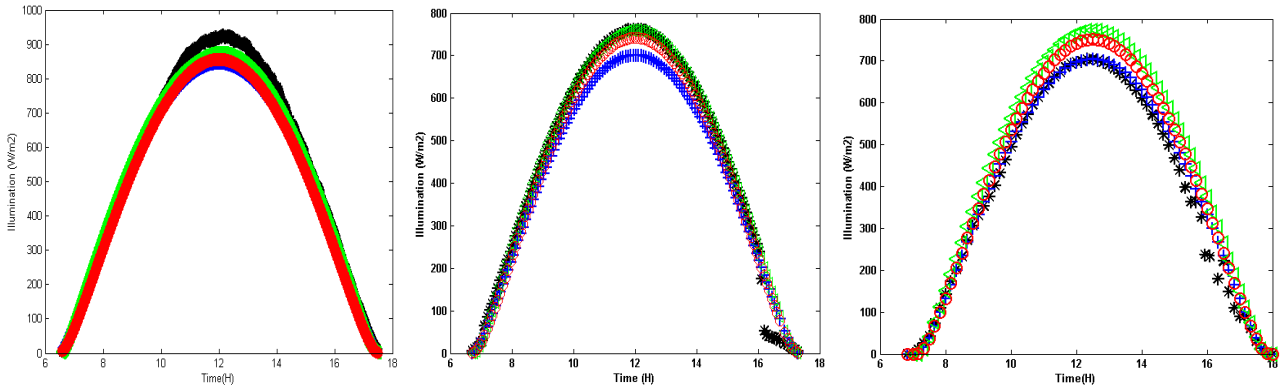

Figure 7. Global solar radiation fluxes on November 13, 2016.

The solar radiation varied over the day, peaking at around solar noon, and has lower values in the case of sunrise and sunset due to the decreased values of solar elevation. Hence, the maximum global solar fluxes reached its maximum value in the middle of 1000 watts per square meter on the duration sun's height, with an increase in the warm months and a reduction in the cold months.

The most obvious finding to emerge from this study is that the statistical results were presented to validate the estimate models with comparison between the predicted and measured values of global solar radiation. Thus, the statistical scores of global solar radiation were calculated at all three stations located in the south of Algeria. The obtained results are depicted in Tables 5 and 6, and Figures 8 and 9.

Table 5. Statistical scores of MBE, RMSE and R for all days in this study on three locations.

Day	Model	Station 1 (Tamanreset)			Station 2 (Adrar)			Station 3 (El -golé a)		
		MBE (Wh/m^2)	RMSE (Wh/m^2)	R	MBE (Wh/m^2)	RMSE (Wh/m^2)	R	MBE (Wh/m^2)	RMSE (Wh/m^2)	R
January 15	Model 1	39.73	51.07	0.9958	54.86	55.53	0.9996	−19.55	28.56	0.9966
	Model 2	57.96	63.90	0.9959	23.84	24.22	0.9996	−43.28	52.72	0.9968
	Model 3	43.72	51.88	0.9957	40.18	40.34	0.9995	−25.89	39.81	0.9961
February 24	Model 1	78.11	90.66	0.9988	80.95	82.47	0.9996	−30.83	41.47	0.9971
	Model 2	86.85	93.68	0.9989	30.84	32.11	0.9996	−65.79	75.77	0.9968
	Model 3	69.64	79.61	0.9985	49.90	50.26	0.9996	−47.45	61.66	0.9972
March 22	Model 1	63.72	81.30	0.9994	65.89	68.96	0.9995	8.17	15.13	0.9988
	Model 2	67.33	76.89	0.9996	4.26	11.90	0.9995	−0.47	11.47	0.9987
	Model 3	31.66	47.72	0.9990	30.33	31.50	0.9995	6.79	14.39	0.9977
April 25	Model 1	0.45	47.14	0.9971	61.61	64.23	0.9997	35.81	40.51	0.9976
	Model 2	3.33	34.99	0.9976	−15.09	16.40	0.9996	−35.34	39.27	0.9972
	Model 3	−43.36	54.50	0.9965	25.33	25.98	0.9997	1.44	16.02	0.9976
May 12	Model 1	−2.79	46.63	0.9977	31.77	38.18	0.9997	27.72	28.00	0.9999
	Model 2	−0.23	33.70	0.9982	−51.69	52.15	0.9996	−58.70	62.50	0.9999
	Model 3	−51.17	59.66	0.9971	−4.35	7.77	0.9997	−8.22	19.73	0.9999
June 03	Model 1	31.96	53.53	0.9992	48.57	50.76	0.9999	−54.49	58.70	0.9987
	Model 2	33.87	45.06	0.9995	−41.51	42.34	0.9998	−147.99	148.69	0.9984
	Model 3	-18.97	30.65	0.9988	12.63	13.71	0.9999	−91.59	92.42	0.9987
July 29	Model 1	55.64	70.84	0.9990	−2.01	23.91	0.9995	18.11	19.45	0.9998
	Model 2	57.37	65.31	0.9992	−95.11	95.52	0.9994	−76.17	78.41	0.9999
	Model 3	5.98	25.93	0.9986	−39.24	40.32	0.9996	−18.68	22.87	0.9998
August 23	Model 1	55.64	70.84	0.9990	61.34	63.99	0.9999	3.32	10.21	0.9992
	Model 2	57.37	65.31	0.9992	−27.36	27.53	0.9999	−88.54	91.20	0.9990
	Model 3	5.98	25.93	0.9986	21.88	22.22	0.9999	−33.84	37.82	0.9992
September 13	Model 1	27.40	48.27	0.9985	50.61	54.58	0.9993	9.60	23.83	0.9986
	Model 2	25.58	38.02	0.9987	−32.61	33.90	0.9992	−71.28	72.22	0.9985
	Model 3	−11.18	29.02	0.9982	8.70	12.47	0.9993	−30.49	32.61	0.9986
October 17	Model 1	20.90	40.20	0.9986	59.00	60.61	0.9996	22.54	34.53	0.9932
	Model 2	18.56	29.54	0.9988	−10.79	12.09	0.9996	−45.16	50.20	0.9927
	Model 3	−10.55	25.86	0.9984	17.83	18.36	0.9996	−14.95	25.73	0.9933
November 13	Model 1	40.12	50.04	0.9987	50.81	51.58	0.9999	−20.47	35.79	0.9899
	Model 2	42.43	46.79	0.9988	−0.87	2.50	0.9999	−76.67	80.84	0.9895
	Model 3	20.20	29.06	0.9985	21.06	21.13	0.9999	−51.21	57.01	0.9900
December 16	Model 1	18.26	31.05	0.9981	44.53	44.73	0.9994	−20.29	28.11	0.9954
	Model 2	34.79	39.33	0.9984	13.20	14.18	0.9995	−46.85	54.68	0.9956
	Model 3	19.20	27.90	0.9978	31.07	32.00	0.9993	−28.61	40.21	0.9949

The Figures (8–11) and the Tables (5,6) illustrated the Mean Absolute Percentage Error, Mean Bias Error, Root Mean Square Error, and the scatter plots.

Moreover, the figure 8 showed the scatter plots of daily global solar radiation values in 2016 was considered as the best model in each station. It can be seen that the data are distributed as a collection of points closer to the perfect fit linear line (red), indicating the relation between measured and

predicted values (W/m^2) over the study period at each station. Interestingly, the best model to use for estimation gives the best approximation with the measured data.

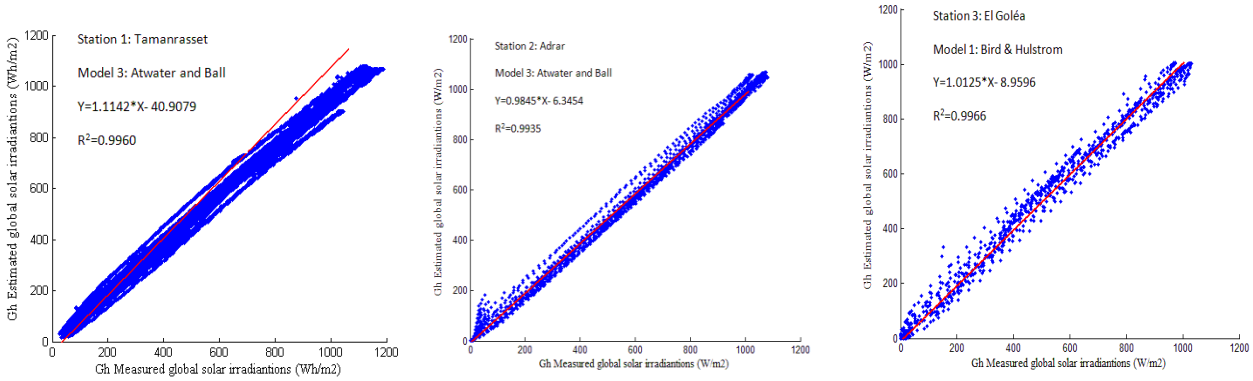

(a) (b) (c)

Figure 8. Scatter plot of the best model at all three stations and over the whole period of study.

As shown in Figures 9–11, the instantaneous global solar radiation predicted by models was presented in good agreement with those computed by all stations.The MAPE recorded at the stations 1 and 2 were less than 10% for all months except for February and July as depicted in Figure 9A,B. However, the MAPE measured at station 3 are less than 20% for all months as shown in Figure 9C. Although the MAPE recorded at stations 1 and 2 are less than 10% and 7%, respectively. The lowest value of MAPE coefficients registered at station 3 is related to the model 1 (MAPE < 8%).

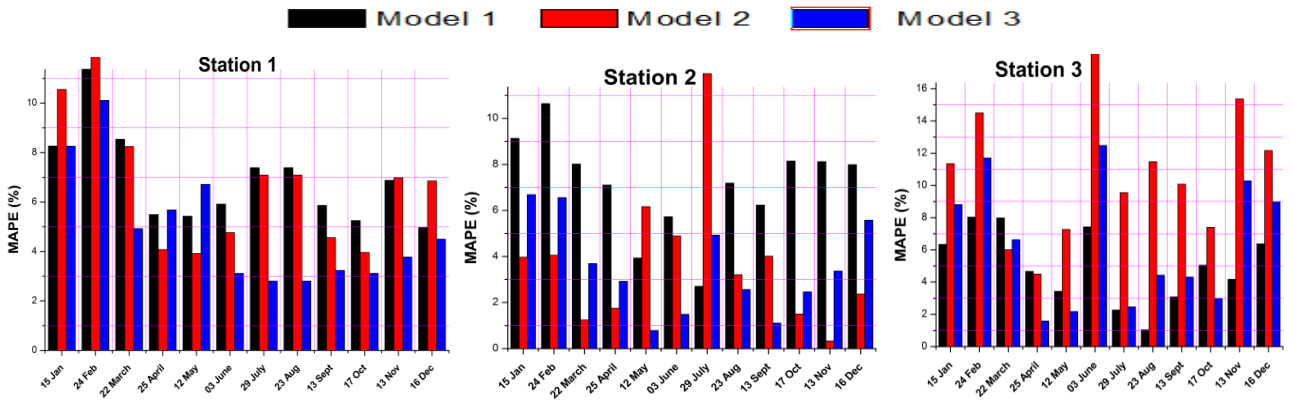

(a) (b) (c)

Figure 9. MAPE over the whole period of study.

Based on the statistical results (rMBE, rRMSE, R), it can be seen that the rMBE results did not exceed 10 and 7% in absolute value for the stations 1 and 2, respectively. The rMBE value of model 1 ranging from −7 to +8% at station 3, and −20 to +13(%) for three models at all station (Figure 10). Therefore, rRMSE did not exceed the percentages of 14, 12 and 20%, for the stations 1, 2 and 3, respectively (Figure 11).

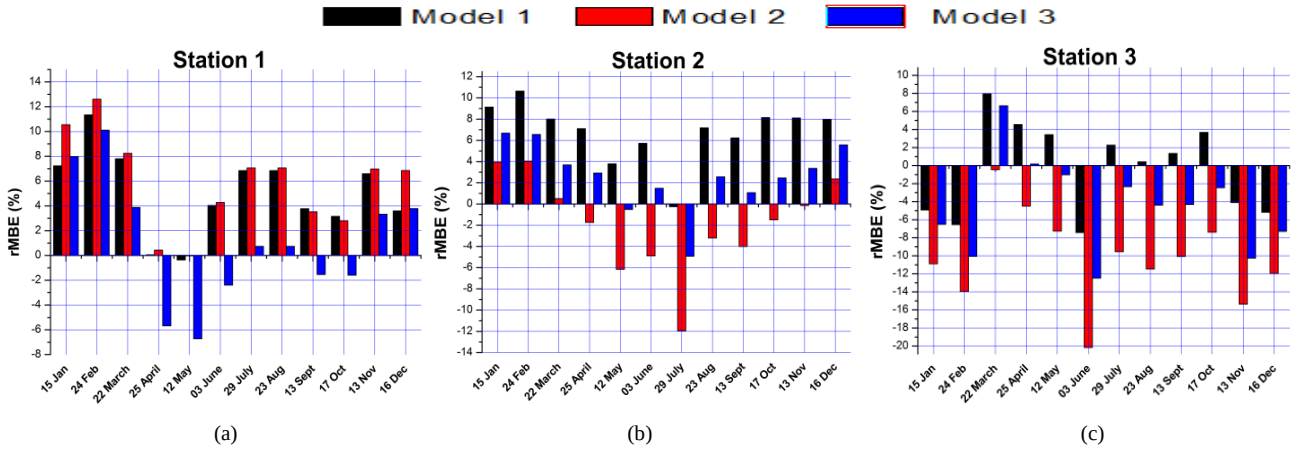

Figure 10. rMBE over the whole period of study.

In this investigation, a good correlation between the predicted and the computed values at each station was appeared; the values of correlation coefficient R are higher than 0.98 as shown in Table 5. The research has also shown that the analysis results of MBE and RMSE have also a good approximation between predicted solar radiation values and those computed by models.

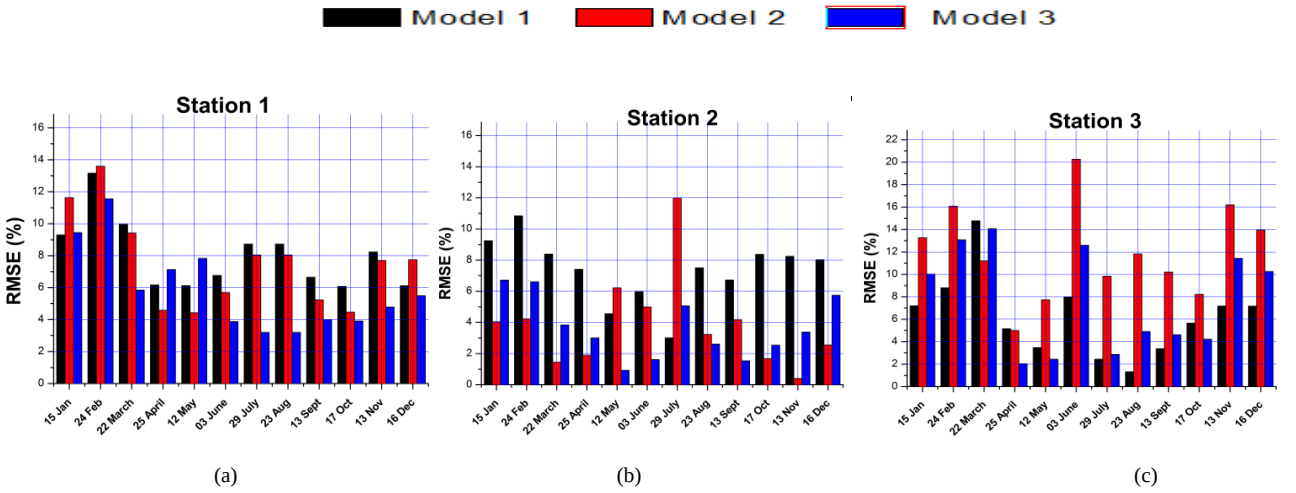

Figure 11. rRMSE over the whole period of study.

The results of statistical of MAPE, MBE, rMBE, RMSE, rRMSE and R for all stations from 1 January to 31 December are reported in Table 6. In general, all models used in this study performed well in estimating global solar radiation. The lowest values of the statistical scores coefficients were in Atwater & Ball model at stations 1 and 2 (MAPE = 4.99 and 3.62, R = 0.9960 and 0.9935, respectively), that indicated that this model is more suitable for the stations 1 and 2 located in Tamanrasset and Adrar, respectively. The statistical indicators values for Bird & Hulstorm model at station 3 have an excellent performance by lower values (MAPE = 4.12, R = 0.9966). It can be concluded that the best prediction model of global solar radiation at station 3 located in El-golé a is the model of Bird & Hulstorm. There is a good correlation between the measured values of solar radiation

and those predicted in the selected stations. The result of this investigation shows that the simulation presents a good agreement with the measured values while the best models gives best results of solar radiation. The errors between the measured and the estimated values are negligible in some cases. Hence, the best studied models have an excellent performance which can be estimate by the global solar irradiance in southern of Algerian.

Table 6. Statistical analysis results.

Station	Model	MAPE (%)	MBE ($Wh/m^2/day$)	rMBE (%)	RMSE ($Wh/m^2/day$)	rRMSE (%)	R
Station1	1	6.87	30.43	4.64	55.98	8.54	0.9953
(Tamanrasset)	2	6.65	37.32	5.69	53.16	8.11	0.9955
	3	4.99	2.44	0.37	42.55	6.49	0.9960
Station 2	1	7.07	50.07	6.74	56.43	7.59	0.9935
(Adrar)	2	4.00	−18.23	−2.45	39.16	5.27	0.9875
	3	3.62	18.78	2.53	30.47	4.10	0.9933
Station 3	1	4.12	−2.87	−0.48	30.59	5.07	0.9966
(El-golea)	2	10.92	−65.41	−10.84	74.84	12.40	0.9938
	3	5.63	−29.89	−4.95	42.89	7.11	0.9941

5. Conclusions

The current study investigated the preliminary assessment of solar energy potential in arid climatic region in the southern region of Algeria. The estimation of the global solar radiation on a horizontal plane under clear sky condition using three empirical models of Bird & Hulstrom, Ashrae and Atwater & Ball were performed. The models were defined with input parameters including the atmospheric-pressure, aerosols scattering coefficient, the average temperature, and the relative humidity.

The performance of these models was performed in three locations: El-golea, Adrar and Tamanrasset using various statistical indicators by comparing the computed and measured values.

The most important results can be concluded as follow:

-The Atwater & Ball model was more suitable for the prediction of global solar radiation in Tamanrasset and Adrar cities. However, The Bird & Hulstrom model provides much better prediction for global solar radiation in El-golea city. The Ashrae model was less accurate than the other models for the whole stations.

-Overall, the relative mean absolute error did not exceed 5% and the coefficient of correlation was greater than 0.99 as well as the relative bias error did not exceed 3%. The relative RMSE was ranged between 4% and 7% for the global irradiation.

-In the clear sky conditions the empirical Atwater & Ball and Bird & Hulstrom models provided the best accuracy for predicting the global solar radiation on a horizontal plane, which are interesting in several solar energy applications (Solar water heating, Solar furnaces and Photovoltaic Cells….etc).

One of the more significant findings to emerge from this study is that this knowledge can help planners and decision makers to make preliminary planning and decide the possible candidate regions for solar power plants, which will be integral for achieving the reduce dependence on fossil fuel-based energy in the future.

Acknowledgments

The authors are grateful to the Research Unit in Renewable Energies in Saharan Medium (RURESM) and laboratory of Energy Environment and Information System (LEEIS), for supporting this research.

Conflict of interest

The authors declare there are no conflicts of interest in this paper.

References

1. Sawin J (2013) Global Status Report. Renewables. REN21 Secretariat, Paris, France.
2. Shukl K, Sudhakar K, Rangneker S (2015) Estimation and validation of solar radiation incident on horizontal and tilted surface at Bhopal, Madhya Pradesh, India. *Am-Eurasian J Agric Environ Sci* 15: 129–139.
3. Benatiallah D, Benatiallah A, Bouchouicha K, et al. (2016) Development and modeling of a geographic information system solar flux in Adrar, Algeria. *Int J Sys Model Simul* 1: 15–19.
4. Kumar BS, Sudhakar K (2015) Performance evaluation of 10 MW grid connected solar photovoltaic power plant in India. *Energy Rep* 1: 184–192.
5. Besarati SM, Padilla RV, Goswami DY, et al. (2013) The potential of harnessing solar radiation in Iran: generating solar maps and viability study of PV power plants. *Renewable Energy* 53: 193–199.
6. Elhodeiby AS, Metwally HMB, Farahat MA (2011) Performance analysis of 3.6 kW Rooftop grid connected photovoltaic system Egypt. *International Conference on Energy Systems and Technologies, Cairo, Egypt, CEST 2011*.
7. Kambezidis HD, Psiloglou BE, Karagiannis D, et al. (2016) Recent improvements of the Meteorological Radiation Model for solar irradiance estimates under all-sky conditions. *Renewable Energy* 93: 142–158.
8. Mejdou L, Taqi R, Belouaggadian N (2011) Estimation of solar radiation in the Casablanca area. *International Congress on Renewable Energies and Energy Efficiency*, F ès Morocco.
9. Mesri M (2015) Numerical methods to calculate solar radiation, validation through a new Graphic User Interface design. *Energy Convers Manage* 90: 436–445.
10. Zaatri A, Azzizi N (2016) Evaluation of some mathematical models of solar radiation received by a ground collector. *World J Eng* 13: 376–380.
11. Lealea T, Tchinda R (2013) Estimation of diffuse solar radiation in the north and far north of Cameroon. *Eur Sci J* 9.
12. Mesri-Merad M (2012) Estimation of solar radiation on the ground by semi-empirical models. *Rev Renewable Energies* 15: 451–463.
13. El-mghouchi Y, Bouardi A, Choulli Z, et al. (2014) Estimate of the direct, diffuse and global solar radiations. *Int J Sci Res* 3: 1449–1457.
14. Yettou F, Malek A, Haddadi M, et al. (2009) Comparative study of two models of solar radiation calculation in Algeria. *Renewable Energies Rev* 12: 331–346.

15. Ya ïche M, Bekkouche S (2010) Estimation of global solar radiation in Algeria for different types of sky. *Rev Renewable Energies* 13: 683–695.
16. Gueymard CA (2014) The sun's total and spectral irradiance for solar energy applications and solar radiation models. *Sol Energy* 76: 423–453.
17. Otunla TA (2019) Estimates of clear-sky solar irradiances over Nigeria. *Renewable Energy* 131: 778–787.
18. Ruiz-Arias JA, Gueymard CA (2018) Worldwide inter-comparison of clear-sky solar radiation models: Consensus-based review of direct and global irradiance components simulated at the earth surface. *Sol Energy* 168: 10–29.
19. Scarpa F, Bianco V, Tagliafico LA (2018) A clear sky physical based solar radiation decomposition model. *Therm Sci Eng Prog* 6: 323–329.
20. Kambezidis HD, Psiloglou BE, Karagiannis D, et al. (2017) Meteorological Radiation Model (MRM v6.1): improvements in diffuse radiation estimates and new approach for implementation of cloud products. *Renewable Sustainable Energy Rev* 74: 616–637.
21. Bilbao J, Miguel A (2010) Estimation of UV-B irradiation from total global solar meteorological data in central Spain. *J Geophys Res* 115: D00I09.
22. De Miguel A, Román R, Bilbao J, et al. (2011) Evolution of erythemal and total shortwave solar radiation in Valladolid, Spain: Effects of atmospheric factors. *J Atmos Sol-Terr Phys* 73: 578–586.
23. Bilbao J, Román R, Miguel A (2014) Turbidity coefficients from normal direct solar irradiance in Central Spain. *Atmos Res* 143: 73–84.
24. Yamasoe MA, do Rosário NME, Barros KM (2016) Downward solar global irradiance at the surface in São Paulo city—The climatological effects of aerosol and clouds. *J Geophys Res* 122.
25. Sanchez-Lorenzo A, Calbó J, Brunetti M, et al. (2009) Dimming/brightening over the Iberian Peninsula: trends in sunshine duration and cloud cover and their relations with atmospheric circulation. *J Geophys Res* 114: D00D09.
26. Hinkelman LM, Stackhouse PW, Wielicki BA, et al. (2009) Surface insolation trends from satellite and ground measurements: comparisons and challenges. *J Geophys Res* 114: D00D20.
27. Hatzianastassiou N, Papadimas CD, Matsoukas C, et al. (2012) Recent regional surface solar radiation dimming and brightening patterns: inter-hemispherical asymmetry and a dimming in the Southern Hemisphere. *Atmos Sci Lett* 13: 43–48.
28. Berk A, Bernstein L, Robertson D (1989) MODTRAN: A moderate resolution model for LOWTRAN7, Rep. GL-TR-89-0122. Air Force Geophys. Lab., Bedford, MA.
29. Bird RE, Riordan C (1986) Simple solar spectral model for direct and diffuse irradiance on horizontal and tilted planes at the earth's surface for cloudless atmospheres. *J Clim Appl Meteorol* 25: 87–97.
30. Gueymard C (1995) A simple model of the atmospheric radiative transfer of sunshine: algorithms and performance assessment. Florida Solar Energy Center.
31. ASHRAE (1985) Handbook of fundamentals. Atlanta, Georgia: American Society of Heating, *Refrigeration, and Air-Conditioning Engineers.*
32. Campbell GS, Norman JM (1989) *An Introduction to Environmental Biophysics*. 2nd ed., New York Springer, ISBN 0-387-94937-2.
33. Atwater MA, Ball JT (1978) A numerical solar radiation model based on standard meteorological observations. *Sol Energy* 21: 163–70.

34. Davies JA (1988) Validation of models for estimating solar radiation on horizontal surface. Atmospheric Environment Service, Downsview (Ont.), IEA Task IX Final Report.
35. Ineichen P (2006) Comparison of eight clear sky broadband models against 16 independent data banks *Sol Energy* 80: 468–478.
36. Bouchouicha K, Razagui A, Bachari N, et al. (2016) Hourly global solar radiation estimation from MSG-SEVIRI images-case study: Algeria. *World J Eng* 13: 266–274.
37. Bouchouicha K, Razagui A, Bachari N, et al. (2015) Mapping and Geospatial Analysis of Solar Resource in Algeria. *Int J Energy, Environ Econ* 23: 735–751.
38. Bailek N, Bouchouicha K, Al-Mostafa Z, et al. (2018) A new empirical model for forecasting the diffuse solar radiation over Sahara in the Algerian Big South. *Renewable Energy* 117: 117–530.
39. Journ é e M, Bertrand C (2011) Quality control of solar radiation data within the RMIB solar measurements network. *Sol Energy* 85: 72–86.
40. Pandey CK, Katiyar AK (2013) Solar radiation: Models and measurement techniques. *J Energy*.
41. Bird RE, Hulstrom R (1981) A simplified clear sky model for directand diffuse insulation on horizontal surfaces, Seri/Tr. 642–761.
42. El-mghouchi Y, El-bouardi A, Sadouk A, et al. (2016) Comparison of three solar radiation models and their validation under all sky conditions—case study: Tetuan city in northern of Morocco. *Renewable Sustainable Energy Rev* 58: 1432–1444.
43. El-mghouchi Y, El-bouardi A, Choulli Z, et al. (2016) Models for obtaining the daily direct, diffuse and global solar radiations. *Renewable Sustainable Energy Rev* 56: 87–99.
44. Bird RE, Huldstrom R (1980) Direct insolation models. *Trans ASME J Solar Energy Eng* 103: 182–192.
45. Stone RJ (1993) Improved statistical procedure for the evaluation of solar radiation estimation models. *Sol Energy* 51: 289–291.
46. National Centers For Environmental Information. Available from: www.ncdc.noaa.gov.
47. Hussain M (1984) Estimation of global and diffuse irradiation from sunshine duration and atmospheric water vapour contents. *Sol Energy* 33: 217–220.
48. Van Heuklon TK (1979) Estimating atmospheric ozone for solar radiation models. *Sol Energy* 22: 63–68.
49. Mefti A (2007) Contribution to the solar deposit determination by solar soil data processing and meteosat images. Doctoral Thesis, University of USTHB Algiers.

AIMS Press